ICANS-XI International Collaboration on Advanced Neutron Sources
KEK, Tsukuba, October 22-26, 1990

Use of a Semi-Opaque Beamstop for Monitoring Sample Transmissions at GLAD*

D. G. Montague,§ J. M. Carpenter, R. K. Crawford, R. Dejus, D. L. Price,
and S. Susman
Argonne National Laboratory, Argonne, IL 60439.
§On leave from Willamette University, Salem, OR.

ABSTRACT

Accurate corrections for many types of measurements made on time-of-flight neutron diffractometers require data on the macroscopic transmission cross-section of the sample used, and this data must span the entire wavelength range covered by the instrument. This report describes a transmission monitor consisting of a semi-opaque beamstop in front of a portion of the array of position-sensitive detectors used for diffraction measurements on the GLAD prototype. The semi-opaque beamstop was made of a molded B_4C-epoxy plate pierced by several small-diameter holes which transmitted a small fraction of the beam, and the segments of the position-sensitive-detectors directly behind these holes served as several independent beam monitors. This arrangement was used on the GLAD prototype flightpath to measure the transmissions of a number of samples, and results of these tests are reported and discussed. Based on these results, a similar transmission monitor has been incorporated in the final GLAD instrument.

I. INTRODUCTION

Accurate corrections for measurements made on neutron diffractometers require data on the transmission cross-section of the samples used. This is necessary because tabulated values of the total cross-sections do not reflect either the sample structure or inelastic scattering, which are unknown until each sample has been completely characterized. This report describes a transmission monitor consisting of a B_4C plate with small diameter holes placed in front of the ^3He linear-position-sensitive detectors (LPSDs) on the prototype flight path for the Glass, Liquid, and Amorphous Materials Diffractometer (GLAD) instrument at IPNS.

*Work supported by U.S. Department of Energy, BES, contract No. W-31-109-ENG-38.

Transmission cross-section measurements are described by Windsor[1] for flat plate samples whose extent is larger than the area of the neutron beam. The process involves the determination of the neutron intensity; that is, background corrected counts in a detector divided by the counts in an incident monitor counter, for a sample in the beam and for the sample out. The attenuation of neutrons by materials in the beam is given by

$$I(\lambda) = I_o(\lambda)\, e^{-\Sigma_i N_i \sigma_i(\lambda) t_i} \tag{1}$$

where the index i represents the various attenuators in the path, such as aluminum windows, gases in the flight path, as well as the sample itself. The symbol $I(\lambda)$ represents the number of counts per unit wavelength, corrected for background, in the downstream detector, normalized for the number of incident neutrons per unit wavelength. Thus when the normalized intensity for the sample in is divided by the normalized intensity for the sample out, we have:

$$\frac{I(\lambda)_{\text{sample in}}}{I(\lambda)_{\text{sample out}}} = e^{-\sigma_T(\lambda) t_s N_s} \tag{2}$$

where N_s and t_s are the number density and thickness of the sample and $\sigma_T(\lambda)$ is the total wavelength-dependent cross-section, scattering plus absorption, of the sample. Then

$$\sigma_T(\lambda) = \frac{1}{t_s N_s} \ln\{I(\lambda)_{out}/I(\lambda)_{in}\} \tag{3}$$

where we have neglected any gas displaced by the sample. In the ideal case[1] the result does not depend on detector efficiency, geometry, or the incident flux distribution. When the sample is not flat or does not cover the entire beam and/or the beam profile is not uniform, the expansion becomes:

$$\frac{I(\lambda)_{\text{sample in}}}{I(\lambda)_{\text{sample out}}} = \frac{\int_{A_1} f(x,y)\, dx\, dy + \int_{A_s} f(x,y)\, e^{-\sigma_T(\lambda) t_s(x,y) N_s}\, dx\, dy}{\int_{A_T} f(x,y)\, dx\, dy} \tag{4}$$

where A_T is the total cross-sectional area of the beam, A_1 the area not obstructed by the sample, A_S the area subtended by the sample, and f(x,y) is the incident neutron beam profile. The length of path through the sample may vary across the sample, depending on the sample geometry. To carry this further, it is necessary to make specific assumptions about the beam profile function f(x,y) and the sample shape $t_s(x,y)$.

II. EXPERIMENTAL ARRANGEMENT

The GLAD instrument recently installed at IPNS is described in a separate report in these proceedings.[2] The prototype flight path used for development of this instrument during 1988-1989,

is also described in that report. This prototype flight path, which was used for the transmission measurements described here, is shown in Fig. 1. The neutrons from the liquid methane moderator were scattered from a sample at 7.7 m from the moderator, and were detected by a detector bank consisting of 55 closely-packed gas-proportional counter LPSDs. Each of these cylindrical LPSDs had a 1.11 cm inside dia x 60 cm active volume, encoded into 64 segments per LPSD. The position identification was accurate to about 1.4 cm, so the data were binned in 2 cm groupings. This detector bank was centered on the direct beam at a position 3.0 m downstream from the sample, and was protected from the full effects of the direct beam by a "beam attenuator" placed just upstream from the detector bank (Fig. 1). This report describes the measurements made with the LPSD segments behind the beam attenuator in the path of the direct beam.

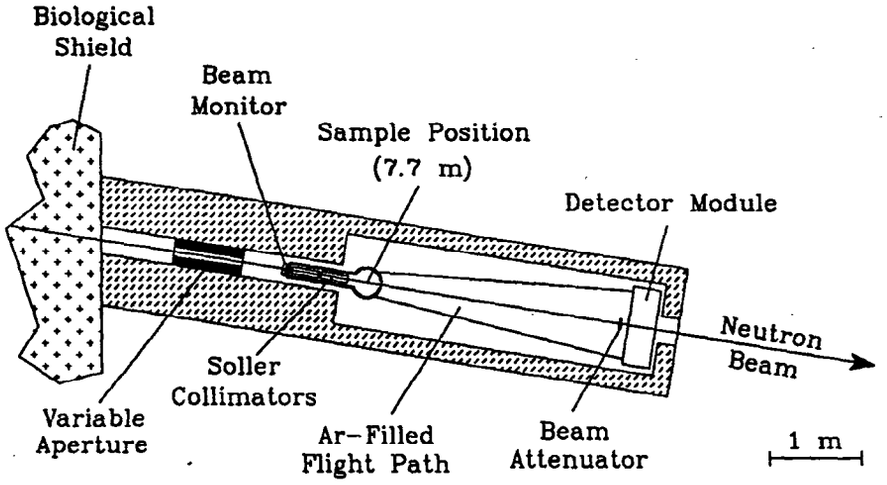

Figure 1. Layout of the prototype GLAD flight path.

There are thermal, epithermal, and higher energy neutrons leaving the moderator "promptly" after the 450 MeV protons strike the target. There are also delayed thermal, epithermal, and higher energy neutrons coming from the moderator with a similar energy spectrum but with essentially no time correlation to the incident proton pulse. This delayed neutron intensity is nearly constant over the full TOF frame.[3,4] Since the soller collimator blades were more-or-less transparent to high-energy neutrons, the penumbra of the high-energy neutrons was primarily determined by the massive apertures upstream from the soller collimators, and was measured to be ~14 cm x 14 cm. The beam divergence permitted by the converging soller collimators determined the much smaller penumbra of the thermal and epithermal neutrons, which was about 4 cm x 4 cm.

The beam attenuator was a slab of natural B_4C, 17 x 17 cm^2 x 1.3 cm thick, with five 0.15 cm diameter holes parallel to the incident neutron beam. The block was made by casting a mixture of B_4C granules and epoxy in a form containing five small rods perpendicular to the face. These holes transmitted enough of the lower-energy neutrons to allow them to be differentiated from the delayed, high-energy neutrons, while keeping the overall count rate sufficiently low to avoid saturating the detection system. This attenuator and its relation to the detector array is shown in Fig. 2. The width and height of the attenuator were chosen to fully cover the penumbra of the high-energy neutrons. The 1.3 cm thickness of the attenuator block was chosen to provide enough attenuation of the medium energies to permit the thermal and epithermal neutrons transmitted

through a pinhole to be discriminated from those transmitted through the absorbing material. (A 1.3 cm thickness of the B_4C-epoxy mix has a transmission of about 5% for neutrons of wavelength 0.1 Å.) The fast delayed neutrons in the incident beam passed through the B_4C beam attenuator with little or no attenuation, but the detectors had low efficiency for detecting these neutrons.

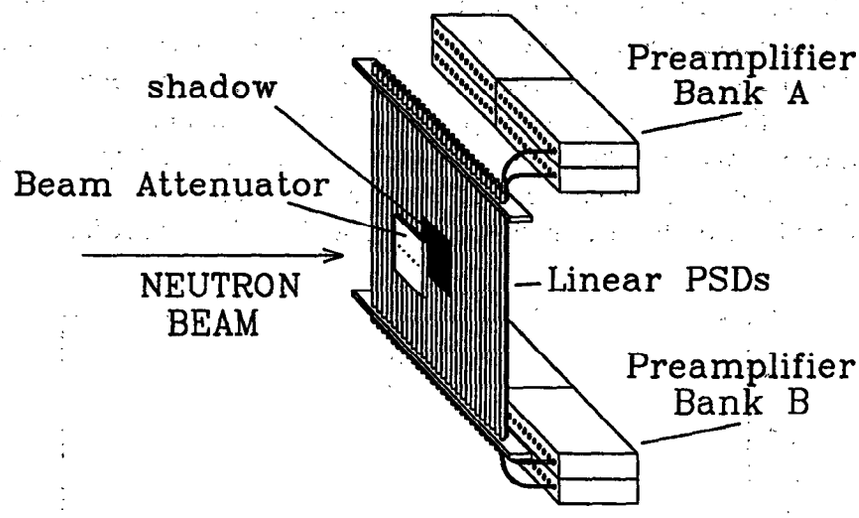

Figure 2. Beam attenuator in front of the detector array.

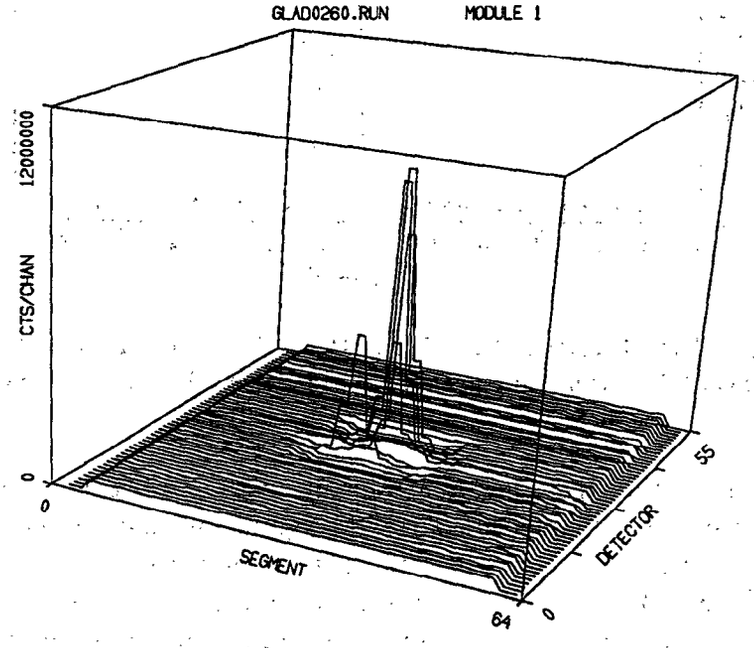

Figure 3. Sum over the time spectra from 200-15000 μs for each segment in the entire 55-LPSD array, with a polyethylene scattering sample. The depressed region in the center is the shadow of the beam attenuator, and the 5 peaks are due to the neutrons transmitted through the pinholes in this beam attenuator, which were in front of 5 of the LPSDs.

III. RESULTS

Figure 3 shows the sum of counts in each segment of the LPSD array for a 0.31 cm thick polyethylene plate sample, with the holes in the beam-attenuator located approximately 0.5 cm below the center line of the LPSD array. All segments of all 55 LPSDs are shown; the vertical scale represents the sums of all counts over the TOF range 200 μs to 15,000 μs. Since the total number of neutrons scattered by the sample into each segment is nearly independent of position, this view shows the shadow of the B_4C beam attenuator as a depressed region at the center of the display. The peaks within this depressed region are due to the neutrons transmitted through the pinholes in the beam attenuator. The LPSDs behind the pinholes have large numbers of counts in the segments near the holes, although the widths of these peaks is much greater than would have been predicted on the basis of the measured detector resolution of 1.4 cm fwhm.

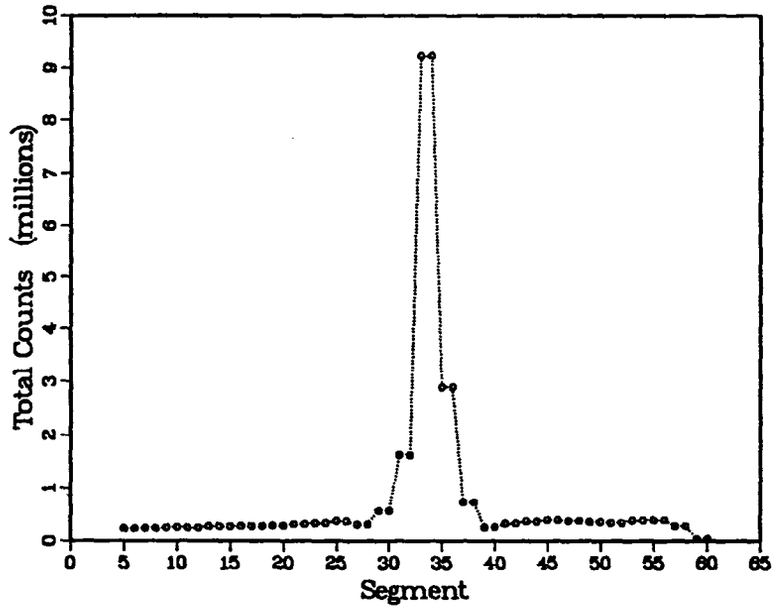

Figure 4. Details of the peak for detector 27 from Fig. 3. The peak is centered behind the pinhole in the beam attenuator in front of this LPSD. Adjacent segments have the same values because of the way the data were grouped.

Figure 4 shows one of these peaks in greater detail. Pairs of adjacent segments were grouped together in the histograming so that separate TOF histograms were collected for each 2-cm-long grouping, and the figure shows the sums over the TOF range of 200 μs to 15,000 μs for each of these groups (as in Fig. 3). Because there were two segments per group and Fig. 4 displays a point for each segment, adjacent points correspond to the same group and thus have the same total number of counts. It can be seen that 6 of the 2-cm-long groups have counts significantly above the surroundings. Examination of the time dependence for each segment of the LPSDs shows that the spread in the position determination is much greater for TOFs near 200 μs than for those longer than 1500 μs. The measured position resolution of 1.4 cm is valid even for the segments behind the pinholes for the longer TOFs, but for these segments for TOFs less than about 600 μs, the high instantaneous intensities lead to pulse-pileup which produces errors in the position encoding, and this is what has led to the broad peaks seen in Figs. 3 and 4. This extreme broadening is not

observed in the segments at the top and bottom of the same LPSDs at the same TOF values, since these segments are not exposed to such high data rates. It appears that the pileup effects have not been large enough to cause data to be lost, so the correct spectrum transmitted through the pinhole can be recovered by summing over all the adjacent groups for which there are significant numbers of counts (6-10 groups, centered behind the pinhole).

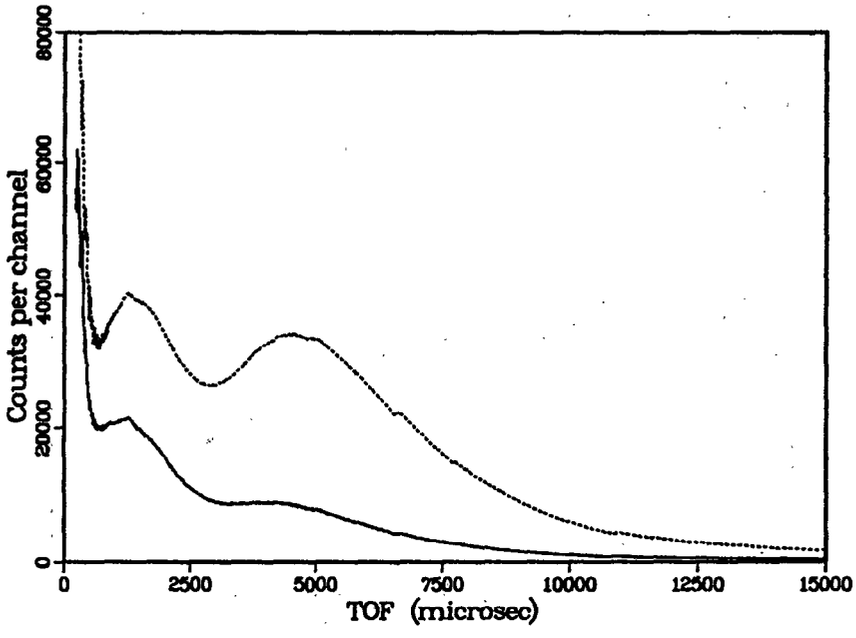

Figure 5. TOF spectra from segments 33-34 of the same LPSD as in Fig. 4. Solid line is for a polyethylene sample, dashed line is for no sample.

Figure 5 gives the time dependence of the counts for the 2-segment group behind the pinhole, which is the one with the most counts in Fig. 4. Data collected with a polyethylene sample (same data as for Figs. 3 and 4) and with no sample are shown. Incident beam monitor data were used to normalize both spectra to the same total number of neutrons incident on the sample position. Since this was a rather thick sample of polyethylene, its transmission was only ~30% as can be seen from the figure. The figure also shows significant distortion of the spectral shape below TOF values of ~1500 μs for both curves. This is due to the misencoding discussed above. Thus such a "single-group" measurement would not be expected to yield accurate sample transmissions at TOF values below ~1500 μs.

As noted above, a more accurate "transmission monitor" can be "constructed" by summing the 10 middle segments of detector 27 (or of any of the other LPSDs behind the pinholes in the beam attenuator). Figure 6 shows a comparison of spectra measured by the incident beam monitor as shown in Fig. 1 and the "transmission monitor" which is constructed by summing the 10 middle segments of detector 29 in a different data run. These measurements were made with no sample in the sample position, and were corrected for the efficiencies of the upstream monitor and the LPSD involved. The agreement is very good for wavelengths longer than 1 Å, except at the longest wavelengths shown, where background subtraction is a problem for the transmission-monitor data. The disagreement below 1 Å is partially due to some penetration of epithermal neutrons through the 1.3 cm thickness of B_4C and epoxy, but may also be due in part to some additional pulse-pileup

effects which result in more extreme position misencoding or in actual detector dead-time. Some of the differences may also be real spectral differences due to the fact that the two monitors were located ~4 m apart along the line of the beam, with the soller collimators, several Al windows, and ~3 m of Ar gas between them.

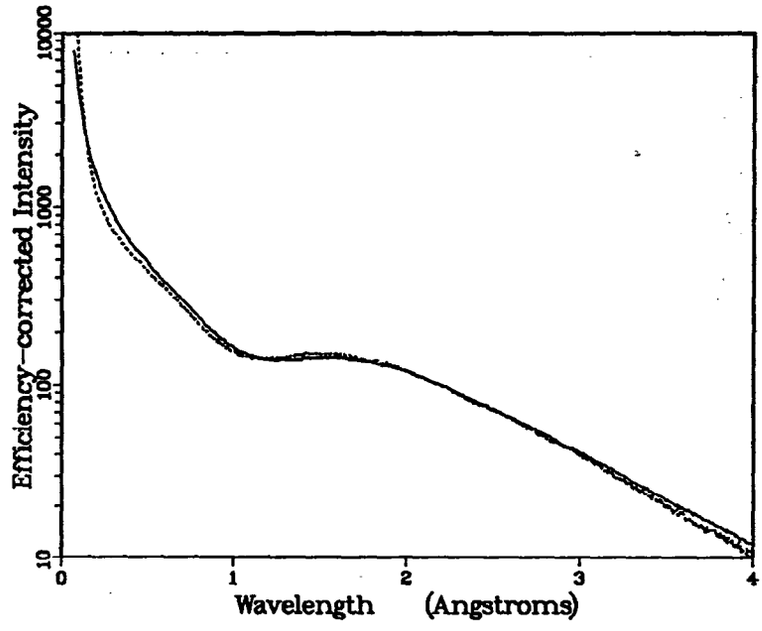

Figure 6. Comparison of the response of the incident beam monitor (solid line) and the transmission beam monitor (dashed line) described in the text. Both have been corrected for their wavelength-dependent detector efficiencies and have been arbitrarily scaled to match near the Maxwellian peak.

In order to correct for the background it is necessary to subtract a term from the intensity for both the sample and the empty sample holder measurements. The long-TOF data from the LPSD segment behind the pinhole were used to determine the delayed-neutron background. The proportion of fast delayed neutrons relative to the thermal and epithermal neutrons of interest changes rapidly with position across the detector bank, since the spatial profile of the former is determined by the upstream beam apertures while that of the latter is determined by the soller collimators. Hence adjacent LPSDs or adjacent segments of the same LPSD which were not behind pinholes could not be used to determine this background. Uncertainty in this background correction currently limits the usefulness of this transmission monitor to wavelengths below ~5 Å.

Figures 7, 8, and 9 show results for transmission cross-sections σ_T measured as a functions of wavelength. Since there were 5 pinholes in the beam attenuator, 5 independent transmission measurements were made concurrently in different LPSDs. Data from 3-5 of these independent measurements are shown in the figures. The solid lines are values from Sears[5] in the case of vanadium and SiO_2, and the values for polyethylene, CH_2, were constructed from H_2O data[6] modified using data from Sears[5]. Errors on the experimental points, calculated using the method of reference 1, are on the order of 2% or less for the vanadium and polyethylene data and somewhat greater for the SiO_2 data. The present measurements yield numbers in reasonable agreement with the cross-sections estimated in this manner. At the long-wavelength end of the measurements a leveling of the measured vanadium cross-section is observed; this is the region of low statistics

beyond 2.0 Å where the background subtraction has the largest effect. For the short-wavelength end the measured cross-section again falls below the tabulated values; this is due to the penetration of neutrons through the B_4C beam attenuator and possibly also to pulse-pileup effects.

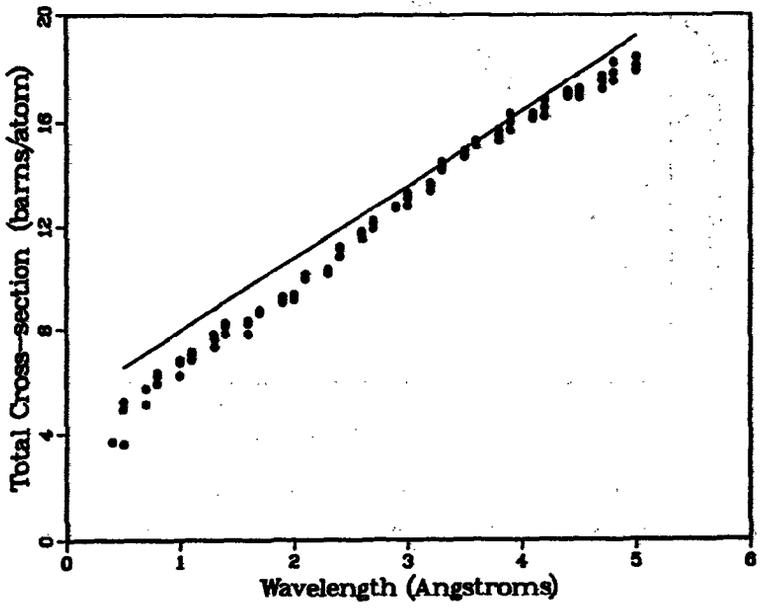

Figure 7. σ_T **for vanadium. The solid circles represent independent concurrent measurements from three of the different LPSDs behind pinholes in the beam attenuator, while the line represents the estimated value.**

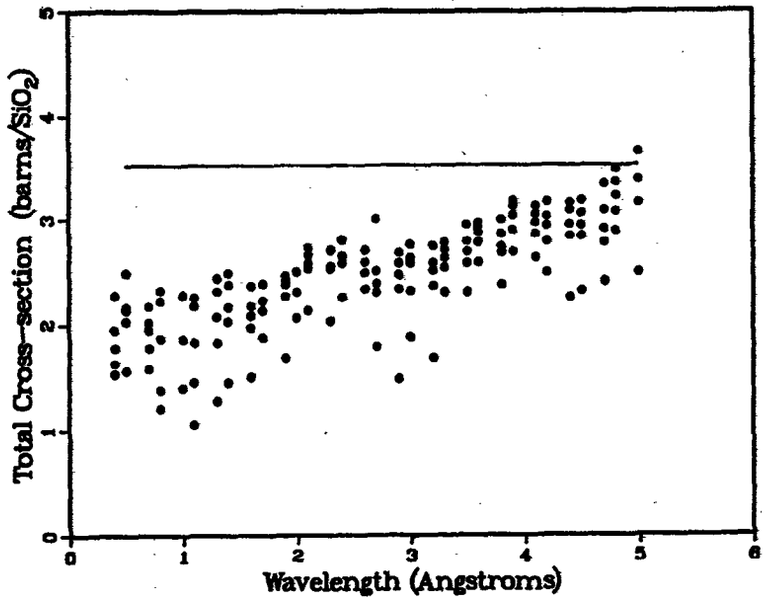

Figure 8. σ_T **for** SiO_2**. The solid circles represent independent concurrent measurements from all five different LPSDs behind the pinholes in the beam attenuator, while the line represents the estimated value.**

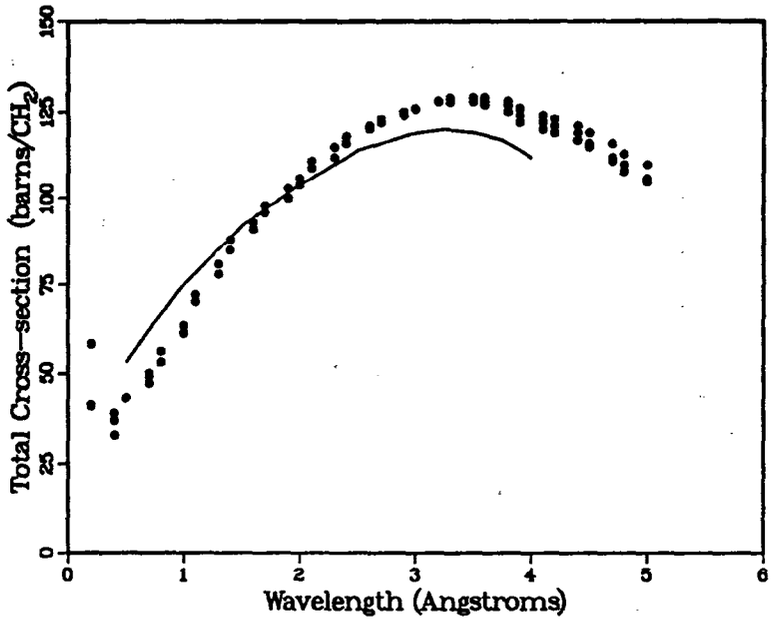

Figure 9. σ_T for polyethylene. The solid circles represent independent concurrent measurements from three of the different LPSDs behind pinholes in the beam attenuator, while the line represents the estimated value.

IV. CONCLUSION

It is seen that reasonable results are obtained from transmission measurements made in the GLAD prototype. Problems still remaining include: (1) Accurate determination of the high-energy neutron background was not possible. (2) The prototype scattering flight path was filled with argon gas with an unknown, and not well controlled mixture of air and water vapor. (3) The count rate was high, especially at short times due to the initial burst of high energy neutrons, leading to pulse-pileup and dead-time effects. (4) The size and shape of the pinholes and the thickness of the B_4C beam attenuator have not yet been optimized. Nevertheless, the method works sufficiently well that a similar "transmission monitor" scheme will be used in the newly-installed final version of GLAD, and development will continue in an effort to reduce the effects of these remaining problems.

References

1. C. G. Windsor. Pulsed Neutron Scattering, Taylor and Francis, London (1981). pp 394-399.
2. R. K. Crawford, J. M. Carpenter, R. Dejus, J. R. Haumann, R. Kleb, D. G. Montague, D. L. Price, and S. Susman. "Status of the New GLAD Instrument at IPNS", these proceedings.
3. J. M. Carpenter. Nucl. Instr. and Meth. 175, 287-292 (1980).
4. J. E. Epperson, J. M. Carpenter, P. Thiyagarajan, and B. Heuser. Nucl. Instr. and Meth. A289, 30-34 (1990).
5. V. F. Sears. Methods of Experimental Physics: Neutron Scattering, vol. 23A, ed. K. Sköld and D. L. Price, Academic Press, Orlando (1986). p 521.

6. D. J. Hughes and R. B. Schwartz. Neutron Cross Sections, 2nd Edition, BNL 325, Brookhaven National Laboratory, Upton, NY (1958).

Q(A.D.Taylor): Are the GLAD detectors in the spectrometer vacuum, or behind a thin window.

A(R.K.Crawford): Detectors are outside vacuum.

Q(R.Pynn): What size pin holes do you use? Could you use this semi-opaque beam stop for TOF SANS measurements?

A(R.K.Crawford): Pinholes are ~0.7 mm dia. In principle this technique can be used for SANS, but in practice detector resolution is usually not good enough to present some cross-talk with the scattering.